

Flux Line Channels and Reduced Hall Effect in Impure 2D Superconductors

Kenneth Holmlund

Department of Theoretical Physics

Umeå University

S-901 87 Umeå, Sweden

Kenneth.Holmlund@TP.UmU.SE

(October 31, 1988; Submitted to Phys. Rev. Lett.)

We have studied the dynamics of flux-lines in an impure two-dimensional superconductor using numerical Brownian dynamics. In the dirty pinning limit and for small center-of-mass velocities the flux lines prefer traveling in narrow channels uniquely determined by the pinning configuration. At a certain critical drag force there is a dynamic transition from this glassy state into a more ordered crystalline state, in which the channel structure vanishes. The channels are studied by monitoring the particle trajectories and the spatial distribution of vortices. By explicitly including a Magnus force in the Langevin equations of motion we induce a Hall field and we find that the effective Hall angle is strongly reduced by the formation of channels, i.e. the channels introduce a transverse energy barrier that guides the motion, predominantly in a direction parallel to the external force. The transverse depinning force is larger than the depinning force in the direction of the drag and thus the Hall field actually vanishes at finite velocities. We propose that the Hall angle can serve as an order parameter for experimental detection of the glass to crystal transition. Our results are in excellent agreement with recent predictions made by Giamarchi and Le Doussal. [1]

The flux line lattice (FLL) of thin film and high- T_c superconductors has been found to exhibit many interesting properties of which the dynamic phase diagram involving both plastic, crystalline, liquid and glassy states is one. [2] In fact this complexity is to be expected since there in the system are four strongly competing energy scales; thermal fluctuations, vortex-vortex interaction, vortex-pinning interaction and the external field. In addition the impurities can be realized in many different ways by varying the density, distribution, range and strength of the interaction potential, in order to model both natural and artificially created impurities.

Much effort has been put into characterizing the nature of the dynamic phase diagram and the dynamic phase transitions. [3,4] This is well motivated effort since to some extent the energy dissipation of the dynamic vortex transitions is responsible for the actual breakdown of the superconducting state.

Koshelev and Vinokour reported computer simulations where they monitored the hexagonal order parameter in order to characterize the phase diagram spanned by the external drag force and the temperature in the presence of pinning. [2] Several attempts have been made to employ perturbative methods in order to compute the center of mass velocity as a function of the external force, but recently Giamarchi and Le Doussal pointed out that perturbation theory in the inverse velocity and disorder breaks down for these systems because some modes of the disorder are not affected by the motion. [1] In addition they also predicted that the vortices should prefer traveling in elastic channels uniquely determined by the disorder configuration. To some extent this prediction was confirmed already before it was made by the

experiments of Träuble and Essmann. [5] Indications of channel-like motion has also been seen in computer simulations of Brass et. al. but then for a system with an interaction potential (Gaussian) far from the true long-range potential and at very low pinning densities. [6]

In this letter we will use the dynamic phase diagram presented by Koshelev et al. [2] as a starting point and inspired by the predictions of Giamarchi et al. [1] we carry on the analysis further.

The starting point is the over-damped (massless) Langevin equation for a vortex i , [7,8]

$$\mathbf{v}_i(t) = \mathbf{F}_d - \sum_{j \neq i} \nabla U_{vv}(\mathbf{r}_{ij}) - \sum_k \nabla U_{vp}(\mathbf{r}_{ik}) - a \mathbf{v}_i(t) \times \hat{\mathbf{z}} + \zeta_i, \quad (1)$$

where U_{vv} is the repulsive vortex-vortex potential, U_{vp} the attractive vortex-pin potential and ζ_i is a noise term satisfying $\langle \zeta_{i,\alpha}(t') \zeta_{j,\alpha'}(t) \rangle = 2T \delta_{ij} \delta_{\alpha,\alpha'} \delta(t - t')$ where α, α' refer to Cartesian components and T is the temperature. \mathbf{F}_d is an external drag force which corresponds to the applied current in the experimental situation and a is a coefficient that governs the strength of the Magnus force (i.e. the fourth term on the l.h.s. is the Magnus force).

The equations of motion are simulated using the method originally described by Ermak [9] and later used for vortices by Brass et. al. [7], using a numerical time step, $\Delta t = 0.1$.

The vortex system is simulated at intermediate magnetic fields, for which the two-dimensional vortex interaction potential is purely logarithmic, $U_{vv}(r) = \ln r/a_0$, [11] where a_0 is the unit measure of length here taken to be the lattice constant of the perfect FLL. This choice of

potential also defines the unit of energy. In practice we use the Ewald summation technique, periodic boundary conditions and the minimum image convention in order to properly handle the long range forces as described by e.g. Frey et. al. [10] The interaction potential used here is somewhat more ambitious than the potential used by Koshelev et al. [2], which was a force shifted logarithmic potential explicitly cut off at $3a_0$ (i.e. not truly long-range). Actually a potential with shorter interaction range more or less just corresponds to a lower magnetic field in the real system. This is due to the peculiar length scale invariant property of the logarithm function. With a full logarithmic interaction all $N_v(N_v - 1)/2$ pair interactions must be taken into account. Thus the present simulations are very much more computationally demanding than would they be if using a short range potential and neighbor lists. In practice it however turns out that the precise choice of interaction potential makes little difference.

The pinning is realized from a set of N_p randomly distributed attractive Gaussian potentials $U_{vp} = -A_p e^{-(r/r_p)^2}$. The parameter set we will consider is: $A_p = 0.006$, $r_p = 0.2$, $N_p = 9500$, $N_v = 20 \times 24 = 480$, $0.005, 0 \leq F_d \leq 0.25$ and for the Magnus coefficient we choose the value $a = 0.2$, i.e. we expect the Hall angle to be $\Phi_H \approx 11.31^\circ$ when the drag force is large enough for the impurities to be neglected (or for a pure system).

The schematic phase diagram sketched in Fig. 1 is by now well established. [2]

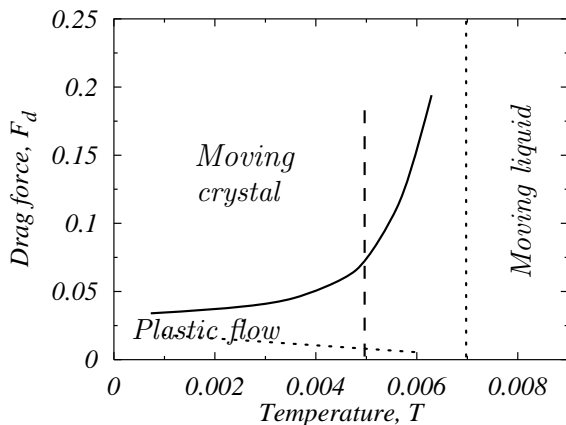


FIG. 1. The dynamic phase diagram of the vortex system. The dashed line starting at $T = 0.005$ and $F_d = 0$ is studied in the simulations. The vertical dotted line at $T = 0.007$ is the absolute melting transition. [12] The lower horizontal (dotted) curve displays the plastic-elastic crossover and the upper curve (solid) shows the transition from from glass-like state into the ordered crystal state.

By varying the drag force F_d , in our simulation we will follow the vertical line starting at $F_d = 0$ and $T = 0.005$.

As also was noted by Koshelev et al. [2] the transition from the glassy state into the more ordered crystalline

phase is sharp. The transition can actually be seen directly in the vortex pair distribution function which is plotted in Fig. 2. The set of curves with smaller amplitudes correspond to drag forces below the transition whereas the set of curves with large amplitudes correspond to forces above the transition. Using this somewhat crude order parameter we determine the transition point to be located at $F_d \approx 0.062$ for this particular pinning configuration.

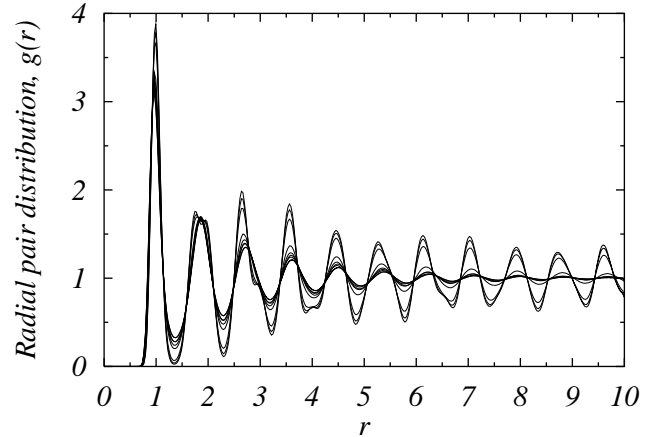


FIG. 2. The dynamic glass to crystal transition is clearly and intuitively visualized by the vortex-vortex pair distribution functions. The set of curves with smaller amplitude correspond to the drag forces $F_d = 0.03, 0.04, 0.05, 0.06$, below the transition, and the curves with larger amplitudes are for $F_d = 0.07, 0.08, 0.1$ above the transition, respectively. The transition occurs at, $F_d \approx 0.062$.

The formation of channels is clearly illustrated in Figs.3 a-d where every 175th configuration out of totally 100000 simulation steps is plotted. This gives a time averaged map of the spatial distribution of vortices in the simulation cell. Each dot represents a vortex and thus the darkest areas are those most favored by the the flowing vortices. The same pinning configuration but different starting conditions were used to produce these plots.

Starting at small forces, $F_d = 0.002$ (Fig.3a), we find that most vortices are pinned to the background and the total flow is almost completely suppressed by the pinning (see also Fig.4). The few vortices that actually do move, creep in channels between the pinned chunks of the lattice. For $F_d = 0.015$ (Fig.3b). the channel structure is clear. Very few vortices are pinned for long times but the mobility is still strongly reduced by the pinning. More close to the transition, for $F_d = 0.05$, the channel structure is still present but the vortices have a tendency to "tunnel" between the channels. Finally for $F_d = 0.08$, above the transition, only a very weak channel structure can be discerned.

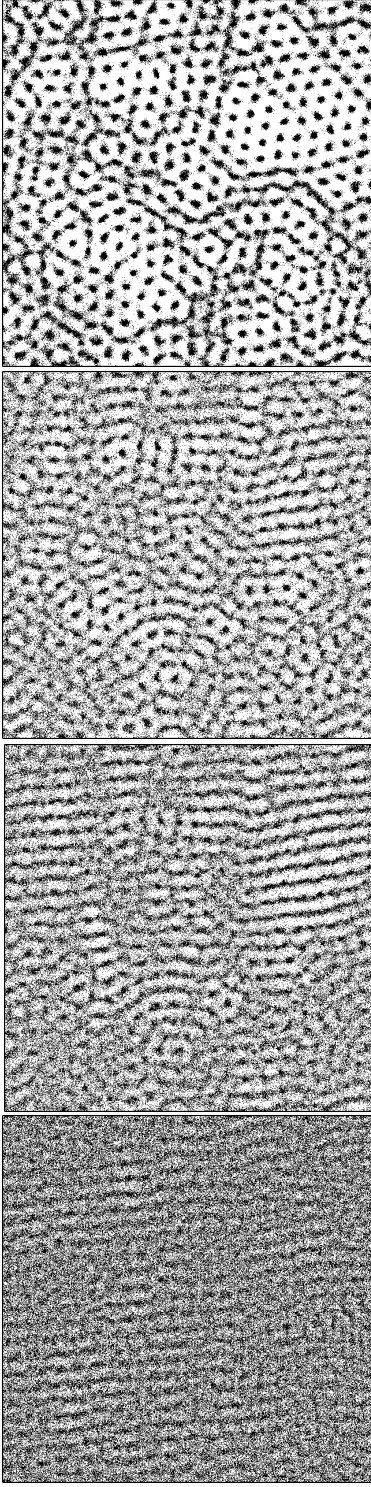


FIG. 3. Time averaged density maps show the preferred spots for a vortex and illustrates how the vortices prefer traveling in elastic channels. Figures a) - d) (from top to bottom) correspond to different drag forces, $F_d = 0.002, 0.015, 0.050, 0.080$.

It is clear that the channel structure is indeed unique for each pinning configuration since runs with very dif-

ferent initial conditions eventually end up with the same flow patterns for a given configuration of pins.

The dependence of the transverse and perpendicular center-of-mass velocities with external force (i.e. the IV-characteristics) is plotted in Fig. 4. In the same diagram also the effective Hall angle is plotted and it is clear that the Hall field becomes strongly reduced as soon as the channels start to form. Interestingly enough the angle is slightly reduced even at velocities far into the "Moving crystal" region of Fig.1. These velocity versus force curves have been averaged over 15 or more realizations of the disorder.

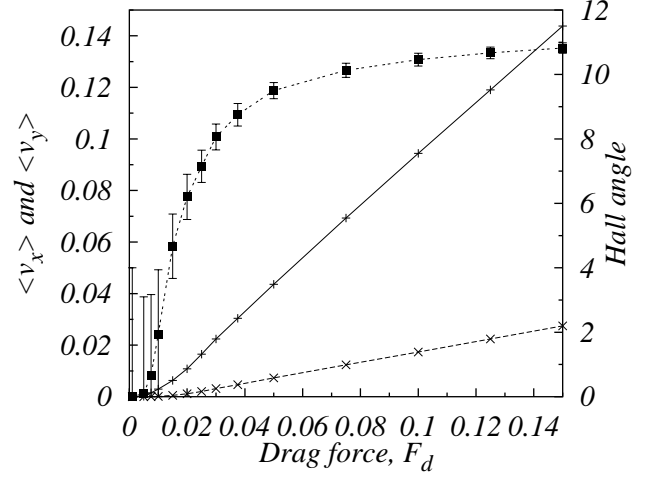


FIG. 4. The average center of mass vortex velocities in the transverse (broken) and horizontal (solid) directions are plotted as a function of the drag force F_d . The corresponding Hall angle shows that the transverse flow is strongly reduced at low velocities due to the presence of the elastic channels.

The strong dependence of the Hall angle with the drag force should be encouraging for designing experiments since it may serve as an order parameter for the glass to crystal transition. It would also be interesting to make more quantitative comparisons with the real system by applying the empirical Corter-Casimir formulas to the model used here, in order to obtain the correct temperature and magnetic field dependencies. [13,7] It has been argued that the vortex lattice tries to minimize its power dissipation by reorienting in the direction of the drag force. [14] This has not yet been verified neither experimentally nor in simulations although the effect probably is of great importance.

The glass to crystal transition is very sharp in the structural and geometrical order parameters and should therefore be accompanied by a strong buildup of wash-board modes, i.e. harmonic components in the center-of-mass velocity. We have preliminary simulational data that verify that not only the fundamental mode but also higher order frequencies are important in the spectrum of the center-of-mass velocity. [15] Coupling of these modes may enhance the strength of the transition and drive the

system into a more ordered state. This and many other issues will be dealt with in a forthcoming publication. [15]

In conclusion we have shown that the flux-lines of a 2D superconductor at low velocities flow in elastic channels that strongly suppresses the Hall field and that the Hall angle vanishes already at finite velocities. The flow patterns are uniquely determined by the pinning configuration.

The author gratefully acknowledges Prof. Petter Minnhagen, Dr. Mats Nylén, Dr. Peter Olsson and Dr. Andrei Shelankov for fruitful discussions. Simulations have been performed on DEC alpha and HP workstations.

-
- [1] T. Giamarchi and P. Le Doussal, cond-mat/9512006.
 - [2] A. E. Koshelev and V. M. Vinokur, Phys. Rev. Lett. **73**, 3580 (1994).
 - [3] For a review see e.g. E. H. Brandt, supr-con/9506003.
 - [4] For a review see e.g. G. Blatter et. al., Rev. Mod. Phys. **66**, 1125 (1994).
 - [5] H. Träuble and U. Essmann, Phys. Stat. Sol. **25**, 395 (1968).
 - [6] A. Brass, H.J. Jensen, and A. J. Berlinsky, Phys. Rev. B **39**, 102 (1989).
 - [7] A. Brass and H. J. Jensen, Phys. Rev. B **39**, 9587 (1989)
 - [8] E. H. Brandt, J. Low. Temp. Phys. **53**, 41 (1983).
 - [9] D. L. Ermak, Jou. Chem. Phys. **62**, 4189 (1975).
 - [10] E. Frey, D. R. Nelson, and D. S. Fisher, Phys. Rev. B **49**, 9723 (1994).
 - [11] W. F. Vinen, in *Superconducting*, edited by R.D. Parks (Marcel Dekker, New York, 1969), Vol. 2.
 - [12] J. M. Caillol et al., J. Stat. Phys. **28**, 325 (1982).
 - [13] See for example: P. G. de Gennes, *Superconductivity of Metals and Alloys*, Benjamin New York, (1966).
 - [14] A. Schmid and W. Hauger, J. Low Temp. Phys. **11** 667 (1973).
 - [15] K. Holmlund, in preparation.